10th ANKARA INTERNATIONAL AEROSPACE CONFERENCE **AIAC-2019-106**
18-20 September 2019 - METU, Ankara TURKEY

INTEGRATED SHAPE OPTIMIZATION OF RAE-M2129 INLET FOR AERODYNAMIC PERFORMANCE AND REDUCED RADAR CROSS SECTION

Tezcan Ünlü[1], Mete Atasoy[2] and Erdem Dinçer[3]
Roketsan Missile Inc.
Ankara, Turkey

Sinan Eyi[4]
Middle East Technical University
Ankara, Turkey

ABSTRACT

Low observability is a key quality of air breathing military aircrafts and the forward observability of such aircrafts are mostly determined by the open ended cavities formed by the air intakes. Geometrical shape of an S-duct intake has effect on both the radar signature indicated by radar cross section (RCS) and the aerodynamic performance indicated by pressure recovery (PR) and distortion coefficient (DC). In this study, shape optimization of RAE-M2129 S-duct inlet is done considering radar signature and key aerodynamic inlet performance parameters by constructing a multidisciplinary optimization cycle. The optimization is carried by a genetic algorithm with dedicated Python scripts generating variable surface shapes using a Bézier curve and running solver tools of computational fluid dynamics and electromagnetics with validated methods.

INTRODUCTION

Air intakes are vital components of aircrafts with air breathing engines and their main purpose is to deliver a uniform stream of air to the engine while maintaining flow qualities for efficient thrust production. Also air intakes play an important role in slowing down the flow for a safe compressor operation. The efficiency of air intakes is crucial such that intakes immensely affect the overall aerodynamic and handling characteristics and capabilities of the aircrafts. There are several types of subsonic inlet configurations used to provide said attributes [El-Sayed and Emeara, 2016]. Aerodynamically, the efficiency of air intakes can be expressed in terms of the pressure recovery (PR), which is affected by the shape of the intake, free stream flow conditions and the engine demands, and in terms of distortion coefficient (DC), which shows the uniformity of the flow at the engine face. Due to the geometrical complexity of the inlet and the high accuracy demand for the aerodynamic coefficients, simulating the phenomena of the flow inside the duct through computational fluid dynamics (CFD) requires special care in the modelling phase. Behaviour of the turbulent flow in the duct can be predicted with Reynolds Averaged Navier-Stokes models with accuracy considering the computational effort.

[1] Engineer, Email: tezcan.unlu@roketsan.com.tr
[2] Engineer, Email: mete.atasoy@roketsan.com.tr
[3] Engineer, Email: erdem.dincer@roketsan.com.tr
[4] Assoc. Prof. Dr, in Aerospace Engineering Department, Email: seyi@metu.edu.tr

When low observability is a desired capability for an aircraft, several aspects concerning surface shape and used materials are needed to be taken into account. The detectability of an aircraft by radar systems can be expressed in terms of radar cross section (RCS) which depends on the frequency band the radar system uses. For a typical jet powered aircraft, it is revealed that for forward observation views, most of the radar waves are deflected back from air intakes [van der Heul, van der Ven, van der Burg, 2006]. In closed cavities like air intakes, high frequency radio waves tend to reflect back to the wave source after multiple reflections. When multiple reflections are taken into account, the energy reflected from a curved duct exits the cavity after more bounces than a straight duct and with the help of coatings and absorbers the scattered energy can be reduced [Brown, 1993].

The objective of this study is to construct a multidisciplinary optimization cycle and to optimize the shape of the M-2129 S-duct [Berens, Delot, Chevalier, Van Muijden, Waaijer and Tattersall, 2012] in terms of RCS while maintaining sufficient aerodynamic performance.

METHOD

CFD Simulations

In CFD analysis, Navier-Stokes equations are solved with Reynolds Averaged Navier-Stokes (RANS) based realizable k-ε turbulence model. Navier-Stokes equation with the most general form is,

$$\boldsymbol{\rho}\frac{\boldsymbol{D\vec{v}}}{\boldsymbol{Dt}} = -\boldsymbol{\nabla p} + \boldsymbol{\nabla \cdot T} + \boldsymbol{\vec{f}} \tag{1}$$

where $\boldsymbol{\rho}\frac{\boldsymbol{D\vec{v}}}{\boldsymbol{Dt}}$ is the overall force on each fluid particle, $-\boldsymbol{\nabla p}$ term is the pressure term, $\boldsymbol{\nabla \cdot T}$ is the stress term and $\boldsymbol{\vec{f}}$ term is the force term acting on the fluid particle.

The Reynolds stress tensor from the Reynolds-averaged momentum equations are as follows,

$$\boldsymbol{R_{ij}} = -\boldsymbol{\rho}\overline{\boldsymbol{u_i' u_j'}} = \boldsymbol{\mu_T}\left(\frac{\boldsymbol{\partial \bar{u}_i}}{\boldsymbol{\partial x_j}} + \frac{\boldsymbol{\partial \bar{u}_j}}{\boldsymbol{\partial x_i}}\right) - \frac{\mathbf{2}}{\mathbf{3}}\boldsymbol{\mu_T}\frac{\boldsymbol{\partial \bar{u}_k}}{\boldsymbol{\partial x_k}}\boldsymbol{\delta_{ij}} - \frac{\mathbf{2}}{\mathbf{3}}\boldsymbol{\rho k \delta_{ij}} \tag{2}$$

Realizable k-ε turbulence model is used to calculate Reynolds stress tensor to satisfy the positivity of normal stress and Schwarz's inequality for Reynolds shear stresses.

Electromagnetics (EM) Simulations

In EM analysis, RCS evaluation methods can be categorized as exact and approximate techniques. Exact techniques solves differential or integral forms of Maxwell equations to evaluate electric fields but are limited to low frequencies, limited by the complexity of the geometry and computationally slow. Approximate techniques uses Physical Optics (PO), Geometric Optics (GO) or a combination of these methods all of which are valid for problems where target size is much bigger than the wavelength. PO method uses the Kirchoff approximation to calculate the total scattered energy in the far field and GO method uses a dense grid of rays that are shot into the object and calculates the RCS by the tracing the rays. A combination of PO and GO methods is the shooting and bouncing rays (SBR) method which is an approximate ray tracing technique used for high frequency problems. SBR method is used for this study as it offers high accuracy levels for high frequency problems and computationally fast. The RCS can be quantified by the power scattered in a direction when an object is illuminated by an incident wave and can be expressed as follows:

$$\boldsymbol{\sigma} = \lim_{\boldsymbol{r\to\infty}} \mathbf{4}\boldsymbol{\pi r^2}\frac{|\boldsymbol{E^{scat}}|^2}{|\boldsymbol{E^{inc}}|^2} \tag{3}$$

where $\boldsymbol{E^{scat}}$ is the scattered electric field, $\boldsymbol{E^{inc}}$ is the incident field at the target and r is the distance from the target the measurement location. The unit for $\boldsymbol{\sigma}$ is dBsm in logarithmic scale. When the transmitting and receiving radar equipment is at the same location, the said system

shows the monostatic RCS of the target but when the receiving equipment is at a different location, the system shows the bistatic RCS of the target.

Optimization Cycle

The constructed optimization cycle includes two sub-cycles for the CFD and RCS evaluations. A parametric Bézier curve is used to generate a solid model to be used in the ANSYS HFSS, a commercial EM solver, for the RCS performance evaluation, and ANSYS Fluent, a commercial CFD solver, for the aerodynamic performance evaluation. Performance outputs for each sub-cycle are used by the genetic algorithm to create design populations with different Bézier curve points to be used to produce following populations. Optimization parameters (Bézier curve points) are selected randomly which evolves with generations according to the Darwin's theory of the survival of the fittest. A schematic of the optimization is provided in Figure 1.

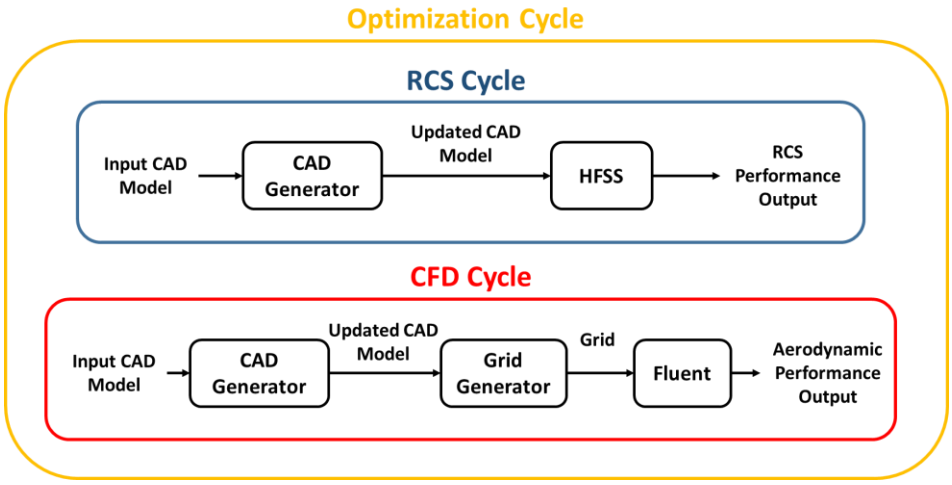

Figure 1: Optimization Cycle Schematic

RESULTS AND DISCUSSION

The analysis tools of RCS and CFD used by the optimization cycles are validated using separate test cases.

EM Simulation Validation

A benchmark model [Escot-Bocanegra, Poyatos-Martinez, Fernandez-Recio, Jurado-Lucena and Montiel-Sanchez, 2008] for the evaluation of RCS is used to validate the approach. The validation case uses a triangular prism as a target (Figure 2). Prism is 200 mm in height and the sides of the triangular base are 167.3 mm, 122.5 mm and 150 mm.

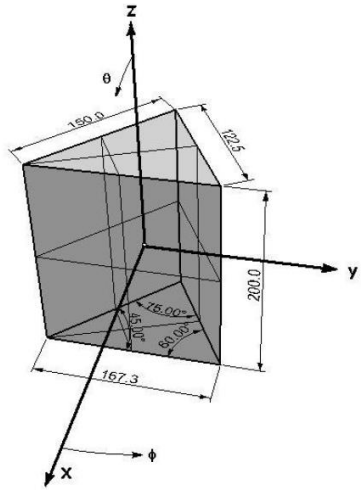

Figure 2: Benchmark Triangular Prism Model

The validation is carried for incident plane waves of $\theta = 90^o$ and ϕ ranging from 0^o to 360^o with 1^o step at 8 GHz for VV polarization. Monostatic RCS values are compared with experimental results (Figure 3).

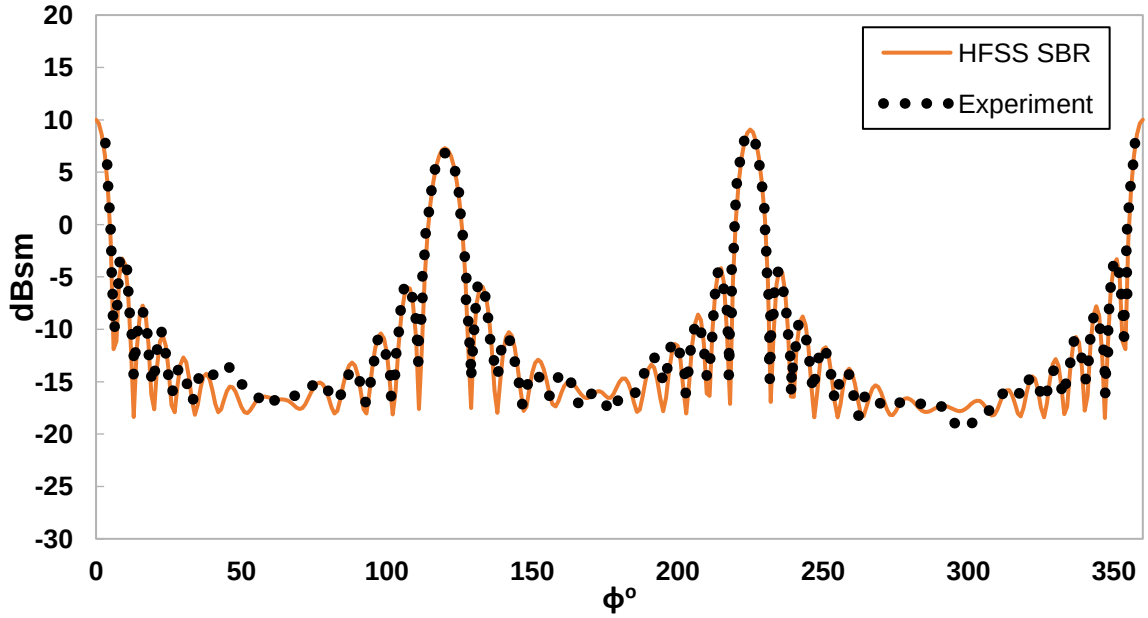

Figure 3: Benchmark Triangular Prism RCS Validation

The comparison shows that the analysis tool HFSS captures the peak RCS values and the diffraction effects caused by the edges of the prism with decent accuracy and can be used in the optimization cycles.

CFD Simulation Validation

A test case of RAE M2129 model with bullet (or engine hub) [Berens, Delot, Chevalier, Van Muijden, Waaijer and Tattersall, 2012] is used validate the CFD approach. The validation case uses an S-duct intake with a circular entry followed by an S bend diffuser (Figure 4).

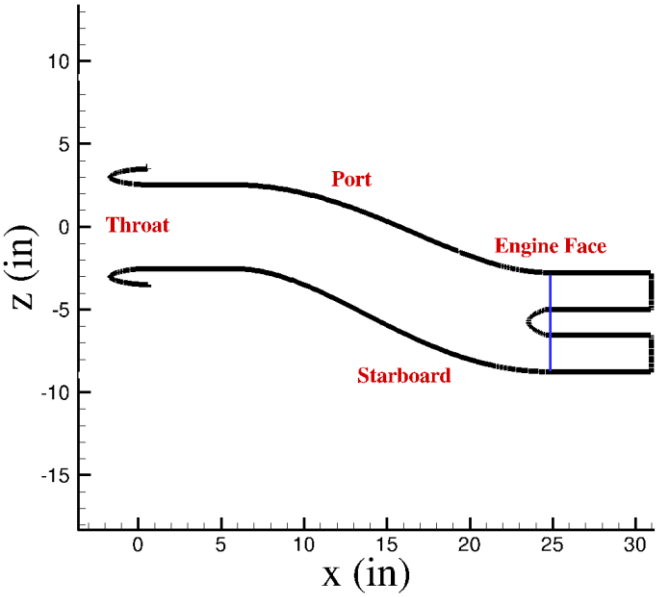

Figure 4: RAE M2129 (with bullet) Model

The steady-state CFD analysis is carried out for the flow conditions summarized in Table 1. with the previously explained method. The obtained results are compared with experimental data in Table 2.

Table 1: RAE M2129 Steady State CFD Analysis Boundary Conditions

RAE M-2129 Model (with bullet) Flow Conditions	
Free Stream Mach	0.204
Free Stream Total Pressure	105139.5 Pa
Free Stream Total Temperature	293.7 K
Incidence	0^o
Side Slip	0^o

Table 2: Steady State CFD Analysis Comparison with Experimental Data

	RAE M-2129 Model (with bullet)	
	Experiment	**CFD Results**
Outlet Pressure (Pa)	-	88500
Mass Flow (kg/s)	2.692	2.720 (1.04%)
Mach Number @ Engine Face	0.4193	0.4232 (0.93%)
Pressure Recovery (PR)	0.9744	0.9790 (0.47%)
Distortion Coefficient	0.313	0.297 (-5.08%)
PRA ($P_{sta\_engine\_face}/P\infty_{tot}$)	0.8522	0.8600 (0.92%)

Wall pressure measurements along the duct are also compared with the experiment, the obtained comparison is provided in Figure 6 and Figure 6 where the starboard side (lower surface) and port side (lower surface) pressure distribution along with the readings from the experiment are shown respectively.

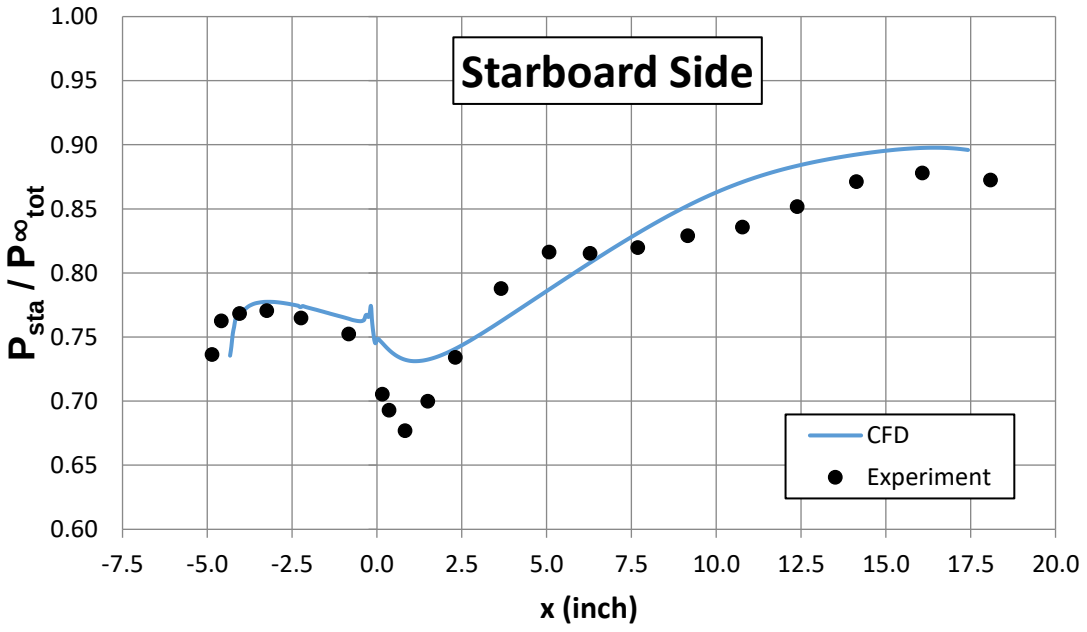

Figure 5: Starboard Side Wall Pressure Comparison

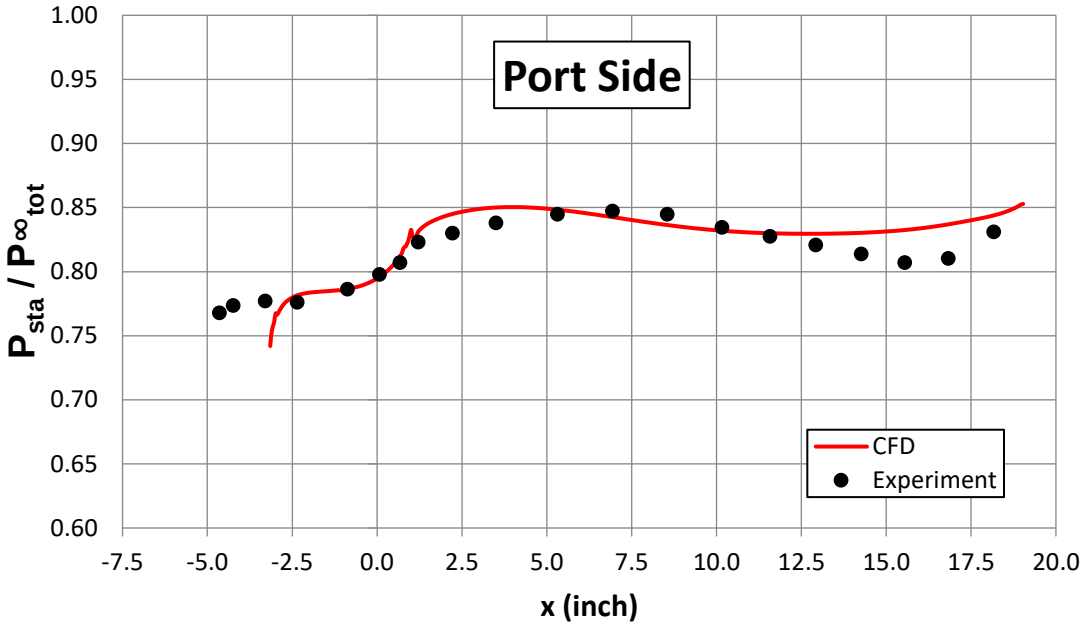

Figure 6: Port Side Wall Pressure Comparison

With the highest difference being the distortion coefficient, flow parameters are within 5% difference margin. Upon this validation RAE M2129 model with bullet is taken as a baseline for the optimization process.

Optimization Inputs, Objectives and Targets

Optimization parameters are the 4 Bézier curve points (control points) that drives the curve generation to be used by the RCS and CFD cycles (Figure 7). The x and y coordinates of these 4 control points (CPs) make up the 8 parameters that are used with the optimization algorithm. The coordinates for the baseline configuration and the limitations for the coordinates are given in Table 3. Optimization objectives and targets for the aerodynamic and RCS outputs are given in Table 4. For the CFD cycles, the same flow conditions with the validation case are used and for the RCS cycle, an incident plane wave perpendicular to the engine throat is shot at 8 GHz for VV polarization which can bounce on surfaces up to 5 times.

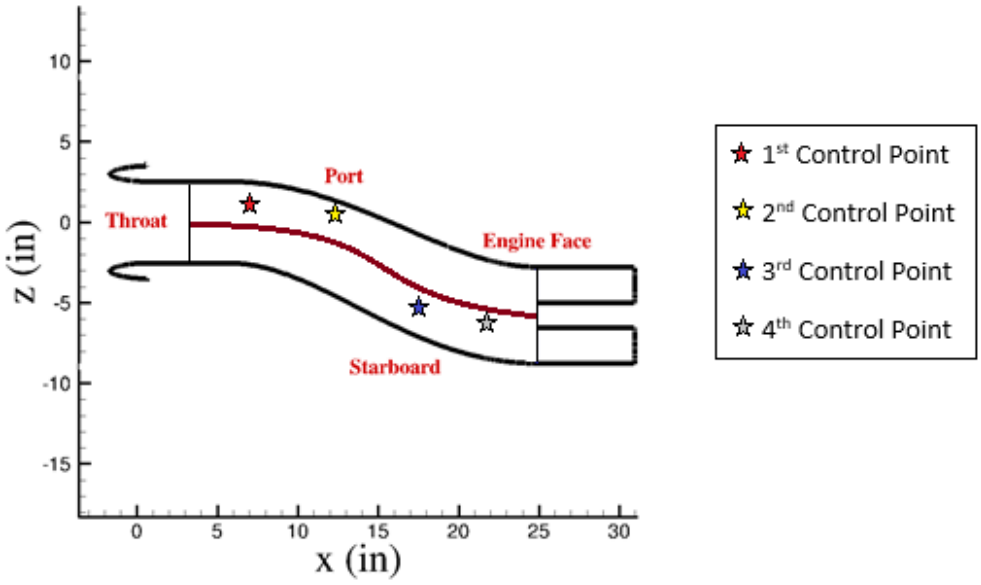

Figure 7: Inlet Curve Points

Table 3: Control Point Limitations

Parameter		Minimum (mm)	Baseline (mm)	Maximum (mm)
CP #1	X	50	65	130
	Y	120	140	160
CP #2	X	180	225	230
	Y	100	125	150
CP #3	X	280	290	320
	Y	-50	15	20
CP #4	X	350	415	420
	Y	0	0	10

Table 4: Optimization Objectives and Targets

Objective	Target
Pressure Recovery (PR)	Maximize
Distortion Coefficient (DC)	Minimize
Radar Cross Section (RCS)	Minimize

Optimization Results

Optimization algorithm assigns fitness values to the individuals in the populations which are calculated by an objective function. The performance of the i^{th} individual is evaluated with the following equation,

$$Performance_i = 0.33 * \frac{PR_i}{PR_{RAE}} - 0.33 * \frac{DC_i}{DC_{RAE}} + 0.33 * \frac{RCS_i}{RCS_{RAE}} \quad (4)$$

Since the nature of the multi-disciplinary problem is unknown, equal valuation is assigned to the optimization objectives with each objective normalized with the baseline RAE-M2129 values. The individuals in the population with the fittest results are retained and used as parents for the new individuals with either mutations or crossovers while the low performance individuals are eliminated. For this study, a population with the size of 30 individuals are generated. The control points of the initial population which includes the baseline RAE-M2129 design is given in Figure 8 with red dotted lines which shows the limitations of the point's design space.

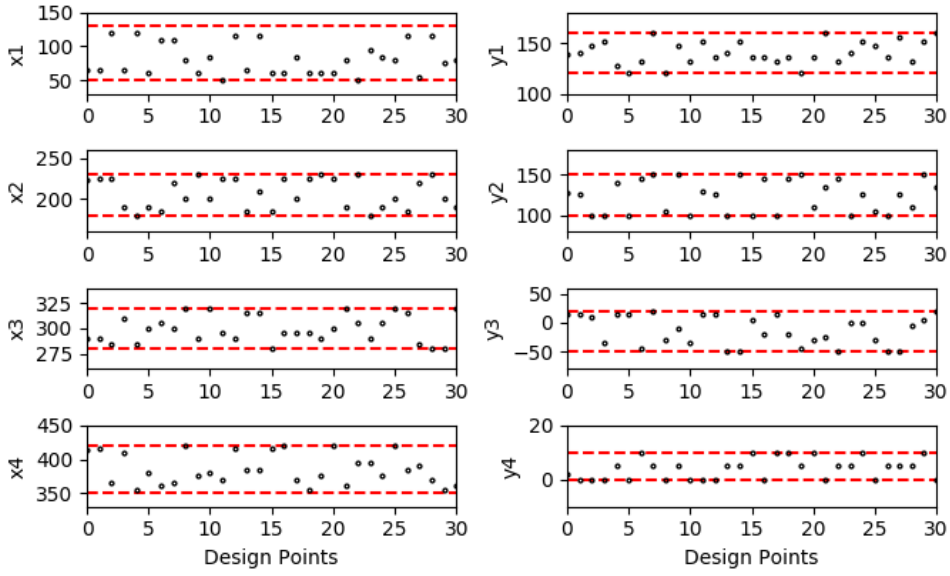

Figure 8: Coordinate Points for the Initial Population

After the generation of the initial population, 15 design points per generation are generated as descendants of the population. The control points of the design history is given in Figure 9.

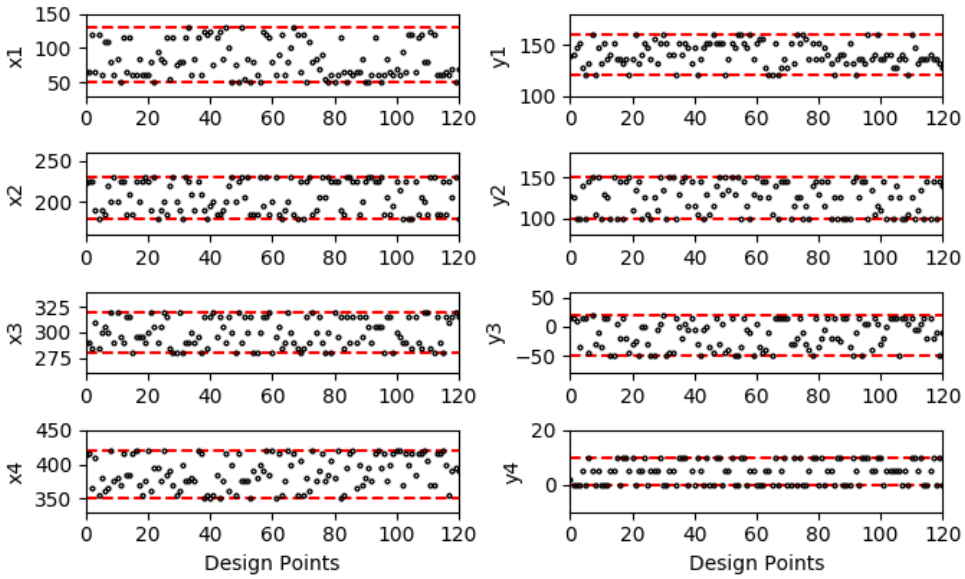

Figure 9: Coordinate Points for the Design History

The initial evaluation of the design space shows that coordinate points are covered well enough for acquiring designs with high performance points. Design history shows that towards the final generations, some control points groups up around certain values with random peaks caused by the randomness of the algorithm. Performance points of the design points through generations can be seen in Figure 10. Performance history shows that after the initial population and 2 generations, algorithm successfully create “descendant” design points with higher performance. Objectives of the optimization is given in Figure 11 and objective values are in line with the performance valuation. Through generations, PR values of the designs increase while the DC and RCS values decrease as intended.

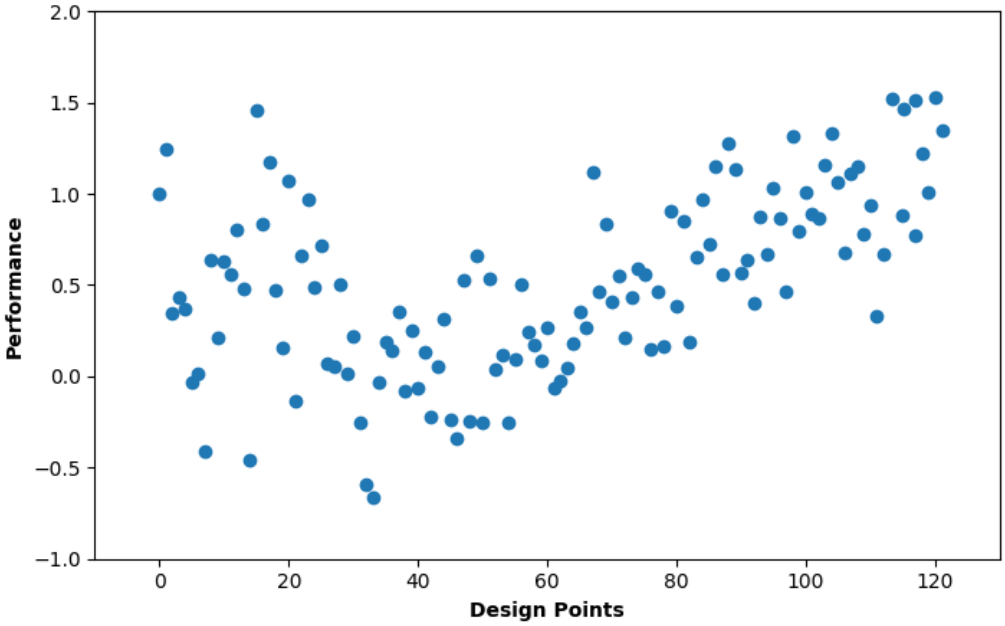

Figure 10: Perfomance of the Design Points

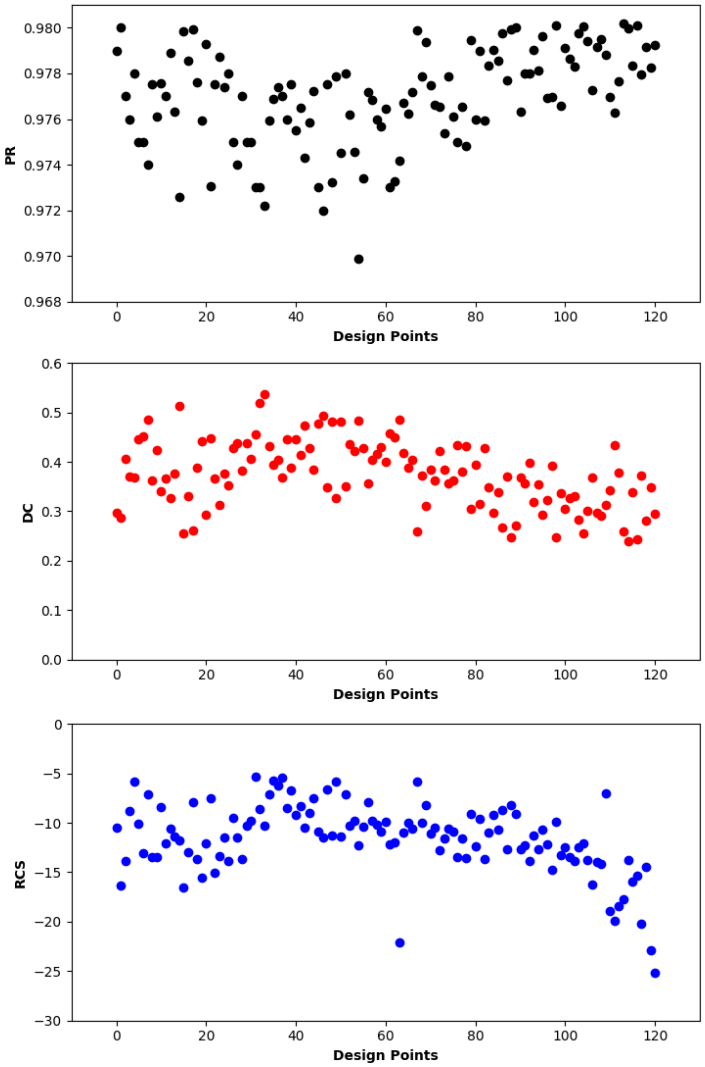

Figure 11: Objective Performance of the Design Points

Correlations between objectives also can be done with the results of the optimization. Correlation plot (Figure 12) shows that PR and DC are heavily correlated, while the colormap reveals that RCS has no correlation with the aerodynamic parameters as expected.

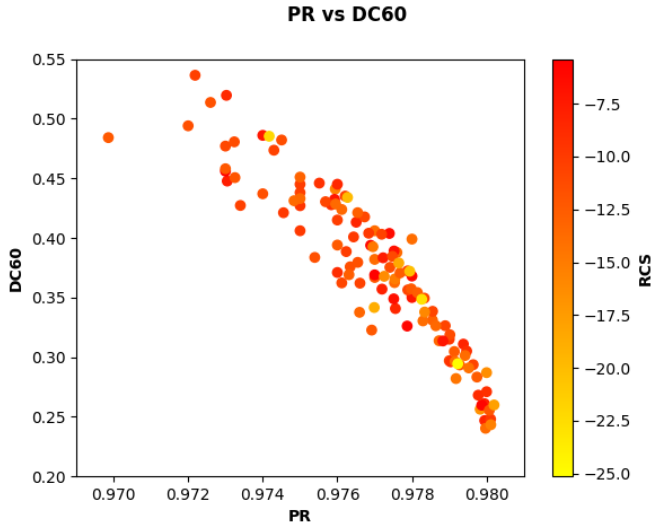

Figure 12: Objective Correlation Plot

The designs with the two highest performance points are Design-119 and Design-113. Comparisons of these designs with the baseline RAE-M2129 design is given in Table **5**. Even though the design with the highest performance is Design-119, Design-113 is selected as the best design because the equal performance valuation of optimization objectives led Design-119 to have the higher performance with the better RCS value. The reason for the similar PR values is that the baseline design already has a good PR value.

Table 5: Comparison of Optimization Designs with the Baseline Design

	RAE-M2129	**Design-113**	**Design-119**
PR	0.9790	0.9802 (+0.12%)	0.9792 (+0.02%)
DC	0.297	0.259 (-12.5%)	0.294 (-0.8%)
RCS (dBsm)	-10.52	-17.74 (-68.6%)	-25.14(-139.0%)

The baseline design and the best design (Design-113) model is given in Figure **13**. The improvement in the RCS values is caused by the change in the part of the surface that the incident plane wave makes the first contact with. As the incident waves are able to bounce up to 5 times, the small change in the inlet surface along with the constant bullet model makes RCS improvements achievable.

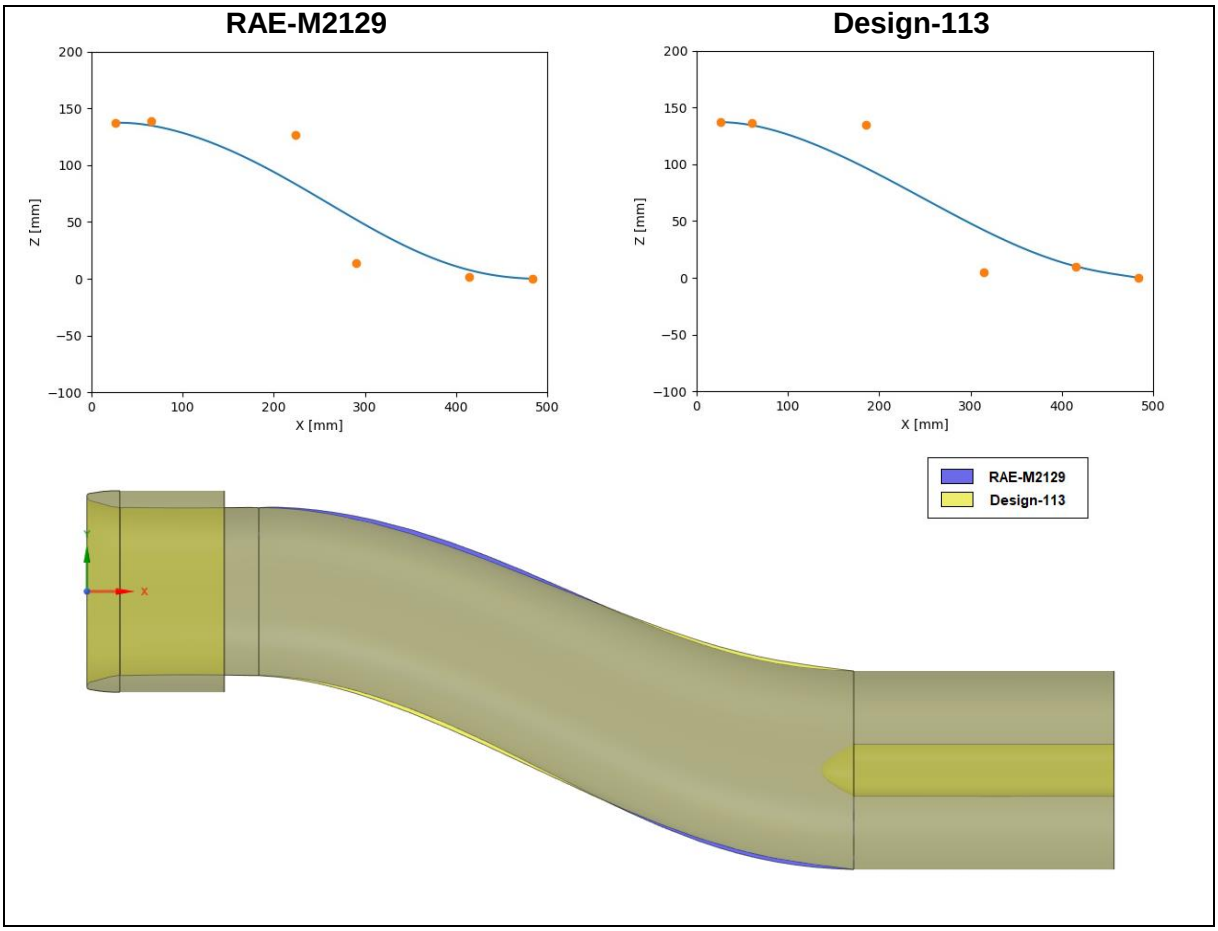

Figure 13: Baseline and Best Model Comparison

CONCLUSION

In this study, shape optimization of an S-duct inlet (RAE-M2129) is done with the consideration of radar signature and aerodynamic performance. An integrated optimization cycle is constructed consisting of an electromagnetic and computational fluid dynamics simulations

with validated methods. The optimization is led by a genetic algorithm which alters the control points of a Bézier curve to generate the optimization inputs. The performance of the individuals in the population are calculated by the optimization objectives, PR and DC for the aerodynamic performance, and RCS for the radar signature. The optimization was carried out by keeping the fittest members of the population with generations and the baseline RAE-M2129 model is improved by reducing the DC by 12 percent and the RCS by 17 percent. This study also showed that the aerodynamic and radar signature performance parameters do not correlate with each other for inlets and a multidisciplinary approach for a design considering aerodynamic performance and low radar signature requires a good evaluation method for performance calculation.

References

Berens, T.M., Delot, A.-L., Chevalier, M., Van Muijden, J., Waaijer, R.A. and Tattersall, P. (2012), *Application of CFD to High Offset Intake Diffusers,* Group for Aeronautical Research and Technology in EURope (GARTEUR), AD/AG-43 Final Report, GARTEUR TP-173, Oct. 2012

Brown, A.C. (1993) *Fundamentals of Low Radar Cross-Sectional Aircraft Design,* Journal of Aircraft, Vol. 30, No. 3, May-Jun 1993

El-Sayed, A.F. and Emeara M.S. (2016) *Intake of Aero-Engines,* The International Conference of Engineering Sciences & Applications, Jan 2016

Escot-Bocanegra, D., Poyatos-Martinez, D., Fernandez-Recio, R., Jurado-Lucena, R. and Montiel-Sanchez, I. (2008), *New Benchmark Radar Targets for Scattering Analysis and Electromagnetic Software Validation,* Progress in Electromagnetic Research, Vol. 88, p: 39-52, 2008

van der Heul, D.R., van der Ven, H. and van der Burg, J.W. (2006), *Full Wave Analysis of the Influence of the Jet Engine Air Intake on the Radar Signature of Modern Fighter Aircraft,* European Conference on Computational Fluid Dynamics, Sep. 2006